Study of the Dielectric Properties of the Perovskite $LaMn_{0.5}Co_{0.5}O_{3-\delta}$

S. Yáñez-Vilar[a], A. Castro-Couceiro[a], B. Rivas-Murias[b], A. Fondado[b], J. Mira[b], J. Rivas[b], and M. A. Señarís-Rodríguez[a]

[a] A Coruña/Spain, Dpto. Química Fundamental, Universidad de A Coruña
[b] Santiago de Compostela/Spain, Dpto. Física Aplicada, Universidad de Santiago

Received January 22nd, 2005; accepted February 25th, 2005.

Abstract. Polycrystalline samples of the charge ordered mixed oxide $LaMn_{0.5}Co_{0.5}O_{3-\delta}$ (T_{CO} = 400 K) have been prepared by the nitrate decomposition method. These samples are biphasic, according to XRPD, and except one, oxygen defficient ($\delta \sim 0.04$-0.05). The study of the dielectric properties of these samples reveal that $LaMn_{0.5}Co_{0.5}O_{3-\delta}$ displays a high dielectric constant, specially at room temperature and low frequencies. This ε'_r is seen to be strongly dependent on the particle size and not so much on the oxygen defficiency and the best properties are found in the sample with biggest particle size (ϕ = 7 μm) for which ε'_r (300 K) $\sim 10^5$ up to $2x10^4$ Hz. Analysis of the role of the grain size and the electrode contacts on the obtained data reveal that this mixed oxide has an intrinsic dielectric constant that is rather high for this type of compounds ($\varepsilon'_{r,\infty} \sim 30$) and that is further enhanced by extrinsic Maxwell-Wagner effects. We relate such enhanced intrinsic dielectric constant to the electronic process of charge ordering present in this material below 400 K.

Keywords: Dielectric properties; Charge ordering; Perovskites

1 Introduction

The discovery of room temperature frequency independent "colossal" dielectric constant in the complex perovskite $CaCu_3Ti_4O_{12}$ [1] has arisen renewed attention in the field of new dielectrics, materials with important applications in many electric and electronic devices, like capacitors [2].

Nowadays, the best industrial performances are given by ferroelectrics [3], i.e., substances with permanent electric dipoles even in the absence of an external electric field, such as the well-known perovskite materials $BaTiO_3$, $PbTiO_3$, etc. [3]. In these materials the ferroelectric state arises because the centre of the positive charges in the lattice is displaced with respect to that of the negative charges. This is, the ultimate origin of this property is structural.

Nevertheless, the possible existence of alternative ferroelectrics with much higher (giant or even colossal) dielectric constants in which that property is based on electronic mechanisms is a very attractive and relevant topic and currently a controversial area [4].

Looking for systems that could be good candidates to display such a property, we focused on mixed oxides that experience charge ordering (CO), i.e., mixed-valent compounds in which the metal ions in different oxidation states order in specific lattice sites giving rise to charge localization. Such materials, that are not new [5], have recently received a lot of attention in connection with the colossal magnetoresistance exhibited by rare earth manganates, some of them with CO [6].

In this context, we carried out the first measurements of capacity and dielectric constant in the CO manganate $Pr_{0.77}Ca_{0.33}MnO_3$, and we found a huge increase of its capacitive response as we approached the temperature at which charge ordering takes place ($T_{CO} \approx 225$ K) [7].

In the search for materials that display a high dielectric constant but at room temperature, we subsequently focused on systems that experience transitions to charge-ordered states at higher and more suitable temperatures, finding very promising results in compounds such as $La_{1.5}Sr_{0.5}NiO_4$ (T_{CO} = 480 K) [8] and $CaMn_7O_{12}$ (T_{CO} = 440 K) [9].

In this paper we report the dielectric behaviour of a related compound $LaCo_{0.5}Mn_{0.5}O_{3-\delta}$, a mixed oxide first prepared in the 1950s to study its magnetic behaviour [10, 11].

From the structural point of view, this compound shows an $A(B_{0.5}B'_{0.5})O_3$ perovskite structure in which two transition metal ions (Co and Mn) occupy the B sites.

According to neutron diffraction -technique that allows to differentiate between the Mn and Co ions -up to 400 K the stoichiometric material adopts a monoclinic structure (S.G.: $P2_1/n$), where the Mn^{4+} and Co^{2+} ions are ordered over the 2b and 2c sites [12]. Above 600 K, the compound shows a rhombohedral structure (S.G.: $R\bar{3}$), where Co and Mn show a site preference for the 1a and 1b sites, repectively. For 600 < T < 400 K the monoclinic and rhombohedral phases coexist [12].

Nevertheless, by means of room temperature powder X-ray diffraction the crystal structure of this compound has been identified as pseudo-cubic [13], orthorhombic [14], or even biphasic with the coexistence of the rhombohedral and orthorhombic phases [15].

This diversity of results is related, on one hand, to the fact that synthetic conditions have a strong influence on the

* Prof. Dr. Mª. A. Señarís-Rodríguez
Departamento Química Fundamental
Facultad de Ciencias
Universidad de A Coruña
E-15071 A Coruña, Spain
Tel: 34 981 167000
Fax: 34 981 167065
e-mail: tonasr@udc.es

 © 2005 WILEY-VCH Verlag GmbH & Co. KGaA, 69451 Weinheim

characteristic (among them, oxygen content) and properties of the studied samples [16]. And on the other hand, to the fact that as the X-ray scattering factors of Co and Mn are similar, these cations can not be differentiated by X-ray diffraction. Therefore, by this technique only a single mixed transition metal (TM) site and an average TM-oxygen distance can be obtained, as opposed to the case of neutron diffraction.

From the magnetic point of view, the oxygen -stoichiometric compound is ferromagnetic, with a $T_C \approx 226$ K, and a magnetization approaching 6 μB. On the other hand, when the compound is non-stoichiometric and oxygen defficiency increases, T_C is seen to decrease and the compound evolves towards a glassy state. And for example, for an oxygen defficiency $\delta \geq 0.025$, the compound has a $T_C \sim 134$ K [16].

From the electrical point of view, this compound shows an electric transition at 400 K that renders it more resistive [17, 18]. This feature has been interpreted on the basis of a charge ordering process between the Co^{2+} and Mn^{4+} ions that would take place at that temperature [17, 18].

2 Experimental Section

$LaMn_{0.5}Co_{0.5}O_{3-\delta}$ samples of different particle size were synthesized by the nitrate decomposition method using La_2O_3, $Co(NO_3)_2{\cdot}6H_2O$ and $Mn(NO_3)_2{\cdot}H_2O$ as starting materials. The procedure was as follows: La_2O_3 was first converted into the corresponding nitrate by dissolution in 30 % nitric acid. This product was then added to an aqueous solution, in which stoichiometric amounts of $Mn(NO_3)_2{\cdot}H_2O$ and $Co(NO_3)_2{\cdot}6H_2O$ were also dissolved. The resulting solution was heated at 200 °C until we obtained a brown resin, whose organic matter was subsequently decomposed at 400 °C. The precursor powders were first treated at 800 °C/21 h, and then pelletized and divided into six groups. Each of these samples was then given different heating treatments for 40 hours at increasingly higher temperatures, namely: 950, 1000, 1100, 1200, 1250 and 1300 °C.

Room-temperature X-ray powder diffraction (XRPD) patterns of all the samples were obtained with a Siemens D-5000 diffractometer and Cu (Kα) = 1.5418 Å radiation. Rietveld profile analysis of the XRPD data was carried out using the Rietica software [19].

The morphology and size of the particles were studied in a scanning electron microscope (SEM), JEOL 6400.

Iodometric titrations were carried out to analyze the oxygen content of the materials. The samples were dissolved in acidified KI solutions, and the I_2 generated was titrated against a thiosulphate solution. The whole process was carried out under an argon atmosphere.

The complex dielectric permittivity of the samples was measured with a parallel-plate capacitor coupled to a precision LCR meter Agilent 4284 A, capable to measure in frequencies ranging from 20 to 10^6 Hz. The capacitor was mounted in an aluminium box refrigerated with liquid nitrogen, incorporating a mechanism to control the temperature up to 350 K. The samples in form of pellets with average diameter of 2 cm were prepared to fit in the capacitor, and gold was sputtered on their surfaces to ensure good electrical contact with the plates of the capacitor. And aware of the controversy regarding extrinsic polarization effects as origin of very high dielectric constants in other ceramic materials [20, 21], additional measurements were performed using both silver paint and sputtered silver contacts.

Also, to test the optimal performance of the experimental set-up, a commercial $SrTiO_3$ sample was measured and values similar to those reported in the literature [22] were obtained.

Impedance complex plane plots were analyzed using the LEMV program [23].

3 Results

3.1 Sample characterization

Rietveld analysis of the room temperature X-ray powder diffraction data indicates that the samples are biphasic in the sense that the mixed Co−Mn perovskite appears under two different symmetries. The majority phase can be indexed on the basis of an orthorhombic symmetry (S.G.: Pnma) [14] and the minority phase on the basis of a rhombohedral symmetry (S.G.: $R\bar{3}c$, in the hexagonal setting) [15]. The so-obtained cell parameters: $a_o \sim 5.8$ Å, $b_o \sim 7.77$ Å, $c_o \sim 5.55$ Å for the majority phase, and $a_h \sim 5.49$ Å, $c_h \sim 13.21$ Å for the minority phase are in good agreement with the data reported in the literature [24].

As for the particle size of the polycrystalline materials, SEM micrographs show that, as expected, the samples that have been annealed at higher temperatures show bigger particle size (Fig. 1). In this context the diameter (ϕ) of the particles increased from 0.3 μm in the sample annealed at a temperature of 950 °C to 7 μm in the sample annealed at 1300 °C (see Fig. 1).

On the other hand, the results of the iodometric tritations indicate that except for the sample annealed at the lowest temperature, that is oxygen stoichiometric, all the other materials show a very similar oxygen defficiency (δ) of 0.04-0.05.

3.2 Dielectric properties

The complex relative dielectric permittivity of the $LaMn_{0.5}Co_{0.5}O_{3-\delta}$ samples,

$$\varepsilon_r(\omega) = \varepsilon_r'(\omega) - i\varepsilon_r''(\omega) \quad (1)$$

($\varepsilon_r = \varepsilon / \varepsilon_0$; where $\varepsilon_0 = 8.85\text{x}10^{-12}$ F/m is the permittivity of free space and ω is the angular frequency) as well as their a.c. conductivity were measured as a function of frequency and temperature.

In what follows we will first describe the results obtained for the sample with biggest particle size ϕ = 7 μm (section i) to then show the influence of particle size (section ii) and the type of contacts (section iii) on the measured dielectric properties.

i) Sample with ϕ = 7 μm

Figure 2(a) shows the real part of the dielectric permittivity ε_r' (the so called dielectric constant) as a function of tem-

 © 2005 WILEY-VCH Verlag GmbH & Co. KGaA, 69451 Weinheim

perature, and obtained at different measuring frequencies. The first remarkable feature is the significant increase of this dielectric constant above a certain temperature giving rise to a very high (giant) dielectric constant at room temperature ($\varepsilon_r' \geq 10^4$ for $\nu \leq 10^5$ Hz), that is 400 times that of the value shown at 77 K.

The behaviour of the dielectric constant as a function of frequency is shown in Figure 2(b). At room temperature, it keeps a constant value above 10^5 up to $2x10^4$ Hz giving rise to a plateau, to then decrease in a step-like manner so that for ε_r' ($\nu \sim 1x10^6$ Hz) $\sim 10^3$. As temperature decreases ε_r' is seen to disminish and so does the extension of the plateau.

On the other hand, the imaginary part of the dielectric permittivity ε_r'' shows rather high values that increase as temperature rises and as frequency decreases (Fig. 2 (c)).

As a result, this sample shows rather high losses as it can be seen in Fig. 2(d), that shows the frequency dependence of the loss tangent, tan $\delta = \varepsilon''/\varepsilon'$, at different temperatures.

The a.c. conductivity ($\sigma_{a.c.}$) of this sample is shown in Figure 3. As it can be seen, this sample is not completely insulating and its $\sigma_{a.c.}$ increases with temperature. In addition, for $T \geq 300$ K the low-temperature $\sigma_{a.c.}$ constant value experiences a sudden increase at $\nu \approx 2x10^4$ Hz, that is in fact the frequency at which the dielectric constant shows the step-like decrease.

ii) Influence of the particle size

We have compared the dielectric behaviour of the samples with different particle size as a function of temperature and as function of frequency and the obtained results are shown in Figures 4 (a-c).

The most remarkable feature is the disminution of various orders of magnitude in the values of ε_r' when the particle size of these polycrystalline materials decreases (Fig. 4(a) and 4(b)). This difference is higher at lower frecuencies and higher temperatures.

On the other hand, the dielectric losses are seen to increase as the particle size of these polycrystalline materials decreases (Fig. 4(c)).

It shoud also be mentioned that, as expected, the a.c. conductivity of these samples is seen to decrease as the particle size decreases (Fig. 4(d)). And the behaviour described for the $\phi = 7$ μm material is found in samples with $\phi \geq 4$ μm.

iii) Influence of the electrode contacts

As indicated in the experimental section we have measured the dielectric permittivity of these samples using different types of contacts. As an example we show in Fig. 5(a) the results obtained on the material with $\phi = 7$ μm using either sputtered gold, either sputtered silver or silver paint contacts. These measurements reveal that at low and medium frequency the type of electrode contact can cause a strong variation of ε_r', and that the highest ε_r' values are obtained when using sputtered gold. Nevertheless at high frequencies ε_r' converges to similar values independently of the electrode contact.

It is also worth pointing out that the samples with sputtered gold are also those that show higher conductivity (Fig. 5(b)).

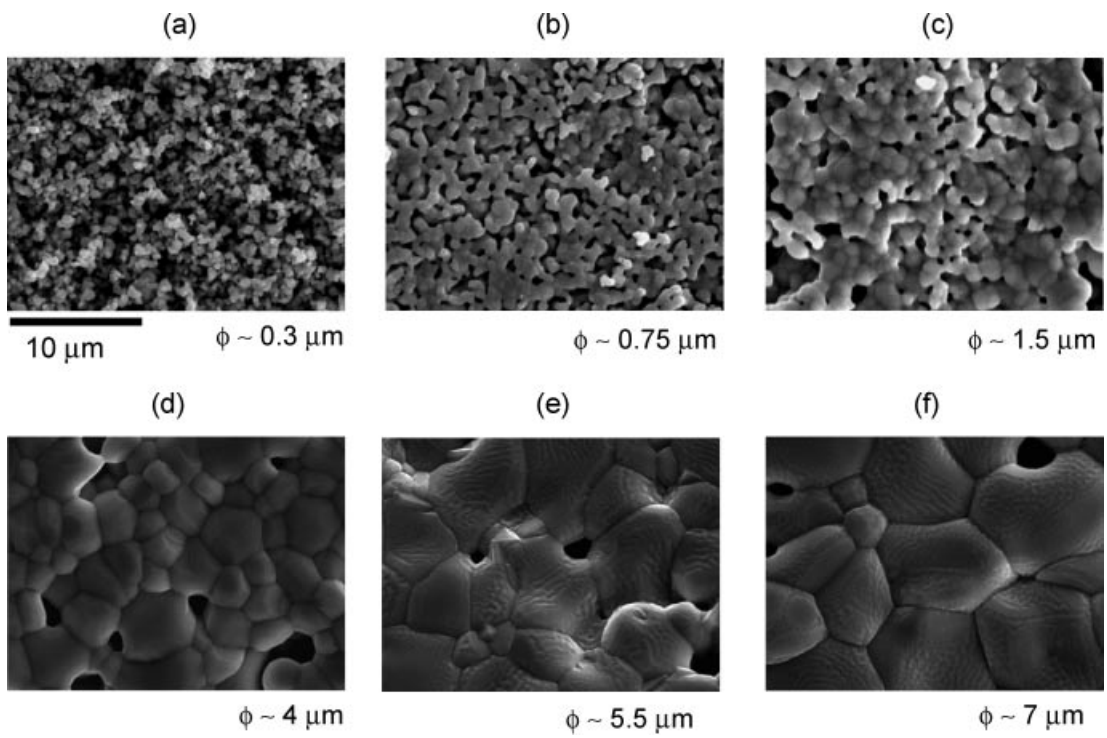

Figure 1 SEM micrographs showing the particle size of the $LaMn_{0.5}Co_{0.5}O_{3-\delta}$ samples annealed at different temperatures: (a)T_{ann}= 950 °C (ϕ~ 0.3 μm); (b) T_{ann}= 1000 °C (ϕ~ 0.75 μm); (c) T_{ann}= 1100 °C (ϕ~ 1.5 μm); (d) T_{ann}= 1200 °C (ϕ~ 4 μm); (e) T_{ann}= 1250 °C (ϕ~ 5.5 μm); (f) T_{ann}= 1300 °C (ϕ~ 7 μm).

 © 2005 WILEY-VCH Verlag GmbH & Co. KGaA, 69451 Weinheim

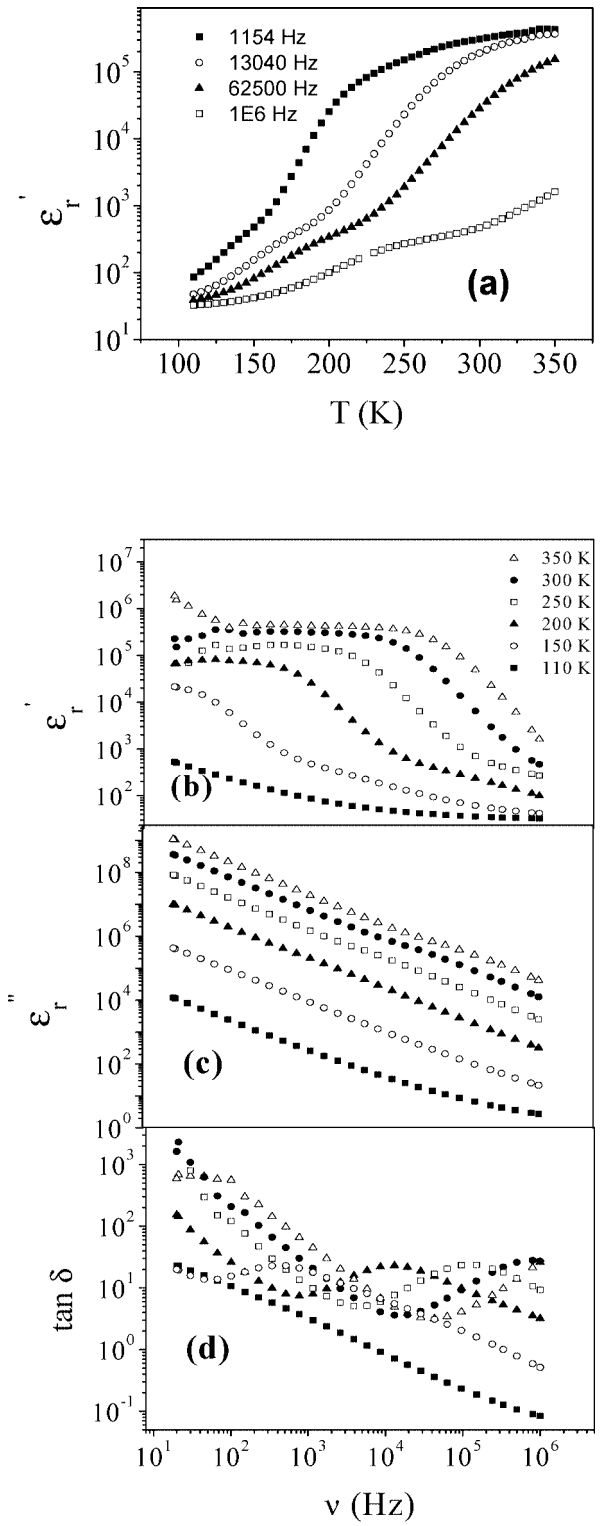

Figure 2 Dielectric behaviour of the sample with $\phi = 7\ \mu m$:
(a) Temperature dependence of the real part of the dielectric constant (ε_r' measured at different frequencies.
(b) Frequency dependence of the dielectric constant at different temperatures.
(c) Frequency dependence of the imaginary part of the dielectric permittivity at different temperatures.
(d) Frequency dependence of the loss tangent measured at different temperatures.

4 Discussion

The obtained results show that $LaMn_{0.5}Co_{0.5}O_{3-\delta}$ displays a very high dielectric constant, specially at room temperature and low frequencies. This ε_r' is seen to be strongly dependent on the particle size of the polycrystalline material and not so much on the oxygen defficiency (that is similar for the samples with $0.75 \leq \phi \leq 7\ \mu m$). Very interestingly the samples with higher particle size are those exhibiting better dielectric properties (higher dielectric constant and lower loss tangent). In this context, for a particle size diameter $\phi = 7\ \mu m$ ε_r' is as high as $5x10^5$ up to $2x10^4$ Hz. This result makes it very attractive for potential applications provided its rather high losses can be minimized.

From the scientific point of view many questions should be understood about the instrinsic or extrinsic nature of the observed interesting dielectric behaviour.

In this context and to study frequency dependent or purely a.c. relaxation effects, we have substracted the d.c. contribution from the observed ε_r'' value, taking into account that [25]:

$$\varepsilon''_{r,die}(\omega) = \varepsilon''_r(\omega) - \frac{\sigma_{d.c.}}{\varepsilon_0 \omega} \qquad (2)$$

where $\varepsilon''_{r,die}$= loss-factor due to a true dielectric response and $\sigma_{d.c.}$= d.c. electric conductivity that is obtained from the extrapolation of the a.c. conductivity, $\sigma(\omega)$, to low frequencies.

The obtained results, corresponding to the sample with highest particle size, are presented in Figure 6. In this representation we see a maximum at very low frequency, that is typical of diffusional processes; and a second maximun at higher frequencies that ressembles Debye-like dipolar relaxation processes with characteristic times, $\tau = 1/\omega$, where ω is the characteristic frequency of relaxation.

A logarithmic fit of the characteristic times versus the inverse of temperature shows an Arrhenius behaviour, $\tau =$

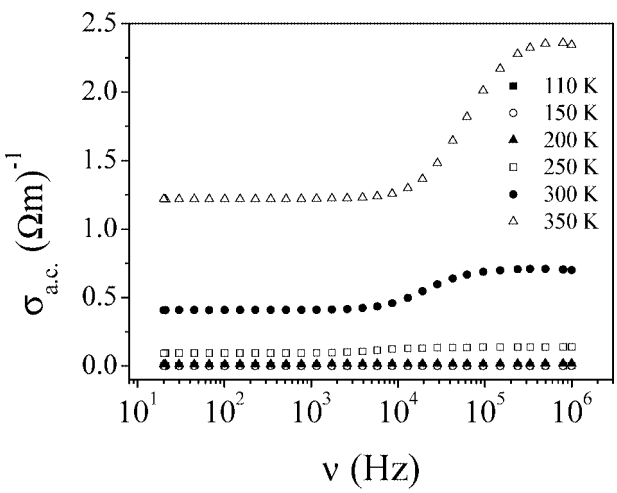

Figure 3 Plot of the a.c. conductivity versus frequency corresponding to the $LaMn_{0.5}Co_{0.5}O_{2.95}$ sample with $\phi \sim 7\ \mu m$ (temperature range: $110 \leq T \leq 350$ K).

 © 2005 WILEY-VCH Verlag GmbH & Co. KGaA, 69451 Weinheim

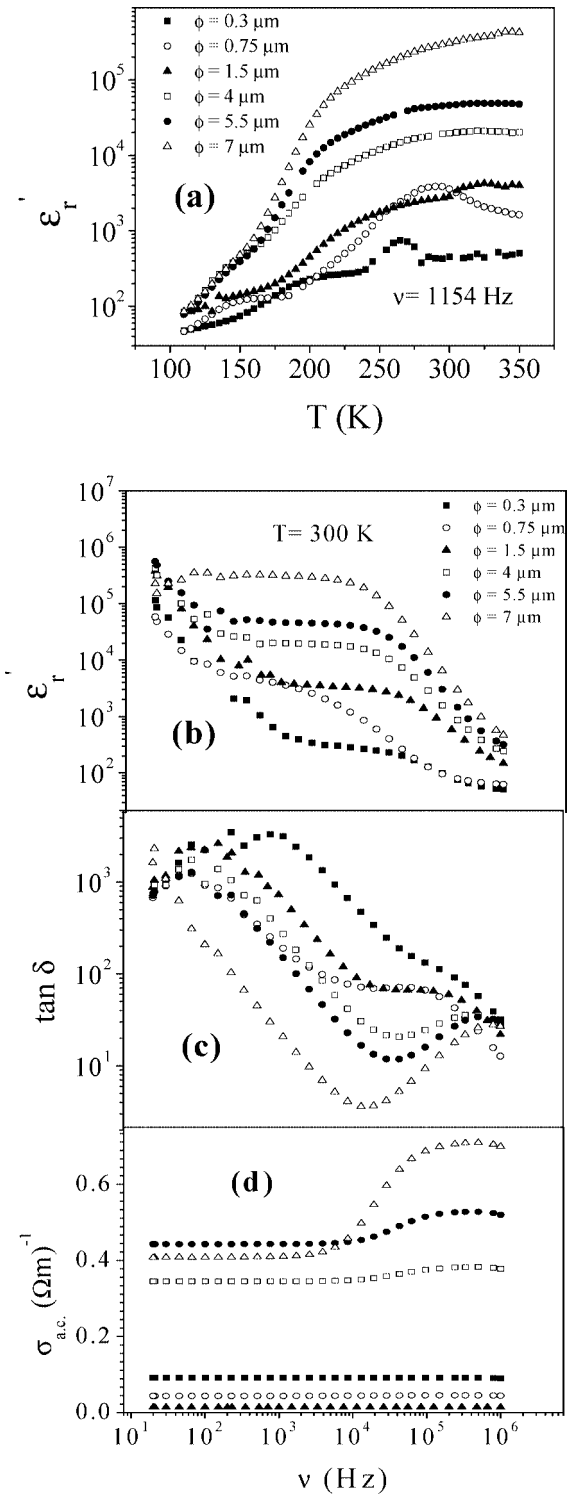

Figure 4 Comparison of the dielectric behaviour of $LaMn_{0.5}Co_{0.5}O_{3-\delta}$ samples with different particle size:
(a) Temperature dependence of the dielectric constant (ε_r') measured at 1154 Hz.
(b) Frequency dependence of the imaginary part of the dielectric permittivity measured at T= 300 K.
(c) Frequency dependence of the loss tangent (tan δ) at T = 300 K.
(d) Frequency dependence of the loss a.c. conductivity at T = 300 K.

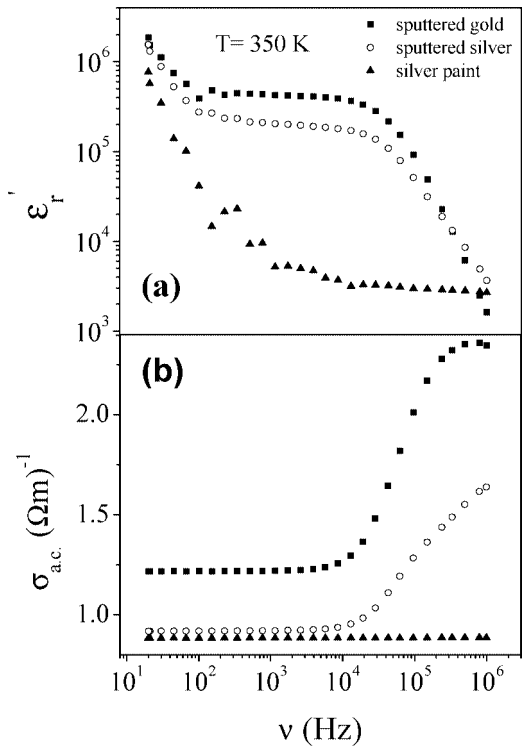

Figure 5 Influence of the electrode contacts on the dielectric and electrical behaviour of the $LaMn_{0.5}Co_{0.5}O_{2.95}$ sample with ϕ = 7 μm at T = 350 K:
(a) Plot of ε_r' as function of frequency.
(b) Plot of a.c. conductivity as a function of frequency.

$\tau_0 \exp(U/(k_BT))$ (where U is the activation energy and k_B the Boltzmann constant) at high temperatures (T > 250 K) with an activation energy U ~ 150 meV.

As for the reasons that would account for the appearance of electric dipoles in these samples, in principle they could have an extrinsic and/or intrinsic origin.

But the observed strong influence of the particle size and the nature of the contacts on their dielectric properties reveal that there is an important extrinsic contribution to the observed high ε_r' values. In this context, the extrinsic interfacial Maxwell-Wagner model [26] allows us to explain the variations observed as the above factors are modified. In this context, for a typical Maxwell-Wagner 2-layer condenser consisting of two parallel sheets of materials (1) and (2), characterized by their dielectric constants, conductivities and thickness ($\varepsilon_{r,1}'$, σ_1, d_1) and ($\varepsilon_{r,2}'$, σ_2, d_2), respectively (Fig. 7), the optic dielectric constant, $\varepsilon_{r,\infty}'$ can be expressed as [27]:

$$\varepsilon_{r,\infty}' = \frac{d\varepsilon_{r,1}'\varepsilon_{r,2}'}{\varepsilon_{r,1}'d_2 + \varepsilon_{r,2}'d_1} \quad (3)$$

and the dielectric constant at low frequencies (the so-called static dielectric constant, $\varepsilon_{r,s}'$) can be expressed as [27]:

 © 2005 WILEY-VCH Verlag GmbH & Co. KGaA, 69451 Weinheim

$$\varepsilon'_{r,s} = \varepsilon'_{r,\infty}\left\{1 + d_1 d_2 \left(\frac{\frac{1}{\sigma_1}\sqrt{\frac{\varepsilon'_{r,1}}{\varepsilon'_{r,2}}} - \frac{1}{\sigma_2}\sqrt{\frac{\varepsilon'_{r,2}}{\varepsilon'_{r,1}}}}{\frac{d_1}{\sigma_1} + \frac{d_2}{\sigma_2}}\right)^2\right\} \quad (4)$$

If the subscript 1 represents the bulk material, that is its intrinsic behaviour, and the subscript 2 comprises factors such as electrode/sample interface and grain boundaries, that is extrinsic factors, and assuming that $\sigma_1 >> \sigma_2$ and $d_1 >> d_2$ and that $\varepsilon'_{r,1} \approx \varepsilon'_{r,2}$ we obtain from eq. (3):

$$\varepsilon'_{r,\infty} \approx \varepsilon'_{r,1} \quad (5)$$

and from eq. (4):

$$\varepsilon'_{r,s} \approx \varepsilon'_{r,1}\left\{1 + d_1 d_2 \left(\frac{\sigma}{d\sigma_2}\right)^2\right\} \quad (6)$$

where σ is the static conductivity of the sample and can be expressed as [27]:

$$\sigma = d\left(\frac{d_1}{\sigma_1} + \frac{d_2}{\sigma_2}\right)^{-1} \quad (7)$$

According to expression (4), an increase in the surface layer, d_2, and a decrease in the sample conductivity gives rise to a decrease of the static dielectric constant as seen in the experimental results when the particle size decreases.

On the other hand, the influence of the nature of the contacts on the ε'_r value can also been understood on the basis of this model. Again, as predicted by the Maxwell-Wagner model in equation (6), as the conductivity of the sample increases when using sputtered gold contacts the dielectric constant is also seen to be higher.

Therefore extrinsic effects play an important role in the observed dielectric behaviour, specially at low frequencies and/or high temperatures.

To try separate the intrinsic and extrinsic contributions we performed complex plane analysis of the obtained data. The best fits were obtained when modelling the impedance spectroscopy (IS) data on the basis of an ideal circuit equivalent consisting of two parallel elements connected in series, one RC element for the bulk, that is frequency dependent, and the other for the grain boundary response. For such a circuit, each RC element gives rise to (ideally) a semicircular arc in impedance complex plane plots, Z'' vs Z' [28]. The number and characteristics of the elements in the equivalent circuit needed to simulate the IS plots depend of the temperature range studied.

In the low temperature range (T< 150 K), the impedance complex plane plots show and arc which intercepts the coordinates origin (Figure 8(a)). This means that at these temperatures and in the frequency range studied only the response due to intrinsic factors is observed.

In the high temperature range (T > 250 K), the impedance complex plane plots show an arc which does not intercept the coordinates origin (Figure 8(b)), which means that only the response due to extrinsic factors is observed.

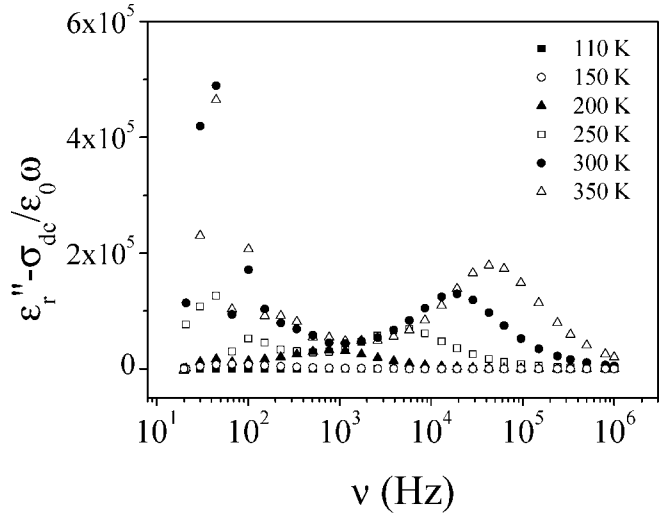

Figure 6 Frequency dependence of the imaginary part of the complex relative dielectric permittivity after substraction of the contribution from free charge carriers in the temperature range 110 ≤ T ≤350 K corresponding to the sample with $\phi \sim 7\,\mu m$.

In the temperature range 150-250 K, the impedance complex plane plots show two arcs (Figure 8 (c)) that can be modeled by the equivalent circuit with two RC elements that we have described before.

The fits using this equivalent circuit indicate that the capacity of the intrinsic bulk response is of the order of pF while that of the interface capacitor is of the order of μF, and that the intrinsic dielectric constant of the compound, $\varepsilon'_{r,\infty}$, is of the order of 30. This $\varepsilon'_{r,\infty}$ is still rather high for this type of oxides, as typical values are $\varepsilon'_{r,\infty} \sim$ 1-10 [29]. And when this enhanced $\varepsilon'_{r,\infty}$ is multiplied by the important contribution of the extrinsic factor it gives rise to the very high dielectric constant measured at room temperature.

Arrived to this point it is interesting to think about the origin of such an enhanced intrinsic dielectric constant for this type of material. In this context it is interesting to note that in our research group we have found high dielectric constants in mixed-oxides with charge ordering, such as in $Pr_{0.67}Ca_{0.33}MnO_3$ [7], $La_{1.5}Sr_{0.5}NiO_4$ [8], $CaMn_7O_{12}$ [9] and $Pr_{2-x}Ca_xMnO_4$ [30] while related members of these families with no charge ordering show much smaller ε'_r values.

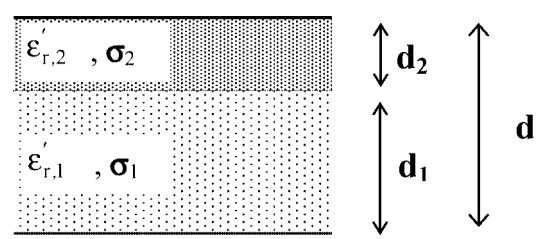

Figure 7 Model of a 2-layer condenser consisting of two parallel sheets of materials (1) and (2).

 © 2005 WILEY-VCH Verlag GmbH & Co. KGaA, 69451 Weinheim

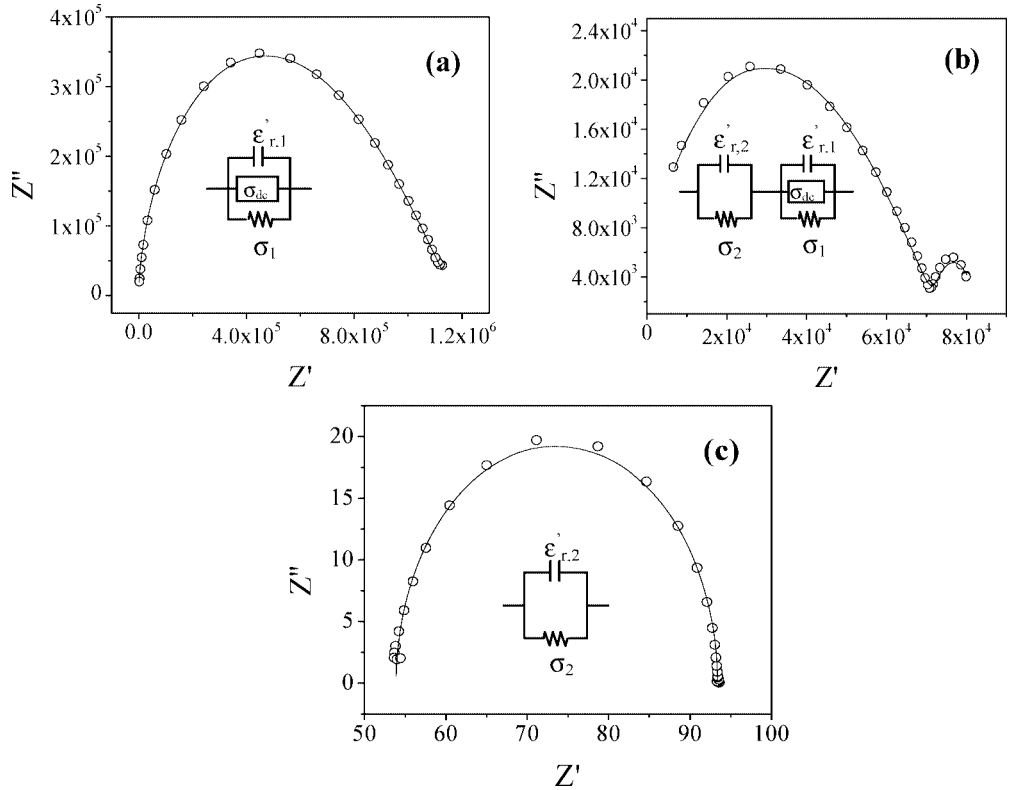

Figure 8 Impedance complex plane plots of the sample with $\phi \sim 7$ μm, corresponding fits and equivalent circuits obtained at differents temperatures: (a) T= 120 K; (b) T= 150 K; (c) T= 300 K. The open circles represent the experimental data and the solid line the corresponding fits.

All these results lead us to associate this enhanced intrinsic dielectric constants to the fact that the charge separation that occurs in a CO transition could lead to the formation of some kind of electrical dipoles in these type of materials, in an analogous way to that theoretically proposed by other authors very recently [31].

More work is in progress to deepen in this very attractive and interesting behaviour.

5 Conclusions

We have prepared polycrystalline $LaMn_{0.5}Co_{0.5}O_{3-\delta}$ samples of different particle size by the nitrate decomposition method. According to X-ray diffraction these samples are biphasic and iodometric titrations indicate that they are oxygen defficient ($\delta \sim 0.04$-0.05), except for the sample annealed at the lowest temperature.

The dielectric properties of this mixed oxide were studied, finding very high values of the dielectric constant specially at room temperature and low frequency, that make it very attractive for potential aplications. This ε_r' is strongly dependent on the particle size of the polycrystalline material and the better properties are found in the samples with bigger particle size. For example for a particle size diameter ϕ = 7 μm ε_r' is as high as $5x10^5$ up to $2x10^4$ Hz.

These high dielectric constants are strongly enhanced by extrinsic polarizations effects, but in any case the value of the intrinsic dielectric constant is already relatively high for such a type of compounds ($\varepsilon_{r,\infty}' \sim 30$).

We relate the enhanced intrinsic dielectric constant of this mixed oxide to the electronic process of charge ordering present in this material below 400 K.

Acknowledgments. We thank financial support of the DGI of the Ministry of Science and Technology of Spain under project FEDER MAT 2001-3749-C02-02 and of the Xunta de Galicia under project PGIDT02PXIC10304PN.

References

[1] M. A. Subramanian, D. Li, N. Duan, B. A. Reisner, A. W. Sleight, *J. Solid State Chem.* **2000**, *151*, 323.
[2] R. J. Cava, *J. Mater. Chem.* **2001**, *11*, 54.
[3] G. H. Haertling, *J. Am. Ceram. Soc.* **1999**, *82*, 797.
[4] P. Lunkenheimer, V. Bobnar, A. V. Pronin, A. I. Ritus, A. A. Volkov, A. Loidl, *Phys. Rev. B* **2002**, *66*, 052105.
[5] E. J. W. Verwey, *Nature* **1939**, *144*, 32 .
[6] C. N. R. Rao, B. Raveau, Colossal Magnetoresistance, *Charge Ordering and Related Properties of Manganese Oxides*, World Scientific, Singapore, 1998.
[7] F. Rivadulla, M. A. López Quintela, L. E. Hueso, C. Jardón, A. Fondado, J. Rivas, M. T. Causa, R. D. Sánchez, *Solid State Commun.* **1999**, *110*, 179.
[8] J. Rivas, B. Rivas-Murias, A. Fondado, J. Mira, M. A. Señarís-Rodríguez, *Appl. Phys. Lett.* **2004**, *85*, 6224.

 © 2005 WILEY-VCH Verlag GmbH & Co. KGaA, 69451 Weinheim

[9] S. Yáñez-Vilar, A. Castro-Couceiro, B. Rivas-Murias, A. Fondado, J. Mira, J. Rivas, M. A. Señarís-Rodríguez, *Z. Anorg. Allg. Chem.* **2005**, *631*, 2192.
[10] J. B. Goodenough, *Phys. Rev.* **1955**, *100*, 564.
[11] J. B. Goodenough, *J. Phys. Chem. Solid* **1958**, *6*, 287.
[12] C. L. Bull, D. Gleeson, K. S. Knight, *J. Phys. Condens. Matter* **2003**, *15*, 4927.
[13] X. L. Wang, M. James, J. Horvat, S. X. Dou, *Supercond. Sci. Technol.* **2002**, *15*, 427.
[14] G. H. Jonker, *J. Appl. Phys.* **1966**, *37*, 1424.
[15] J. B. Goodenough, A. Wold, R. J. Arnott, N. Menyuk, *Phys. Rev.* **1961**, *124*, 372.
[16] R. I. Dass, J. B. Goodenough, *Phys. Rev. B* **2003**, *67*, 014401.
[17] C. L. Bull, R. Mortiemer, G. Sankar, D. Gleeson, C. R. A. Catlow, I. G. Wood, G. D. Price, *Synthetic Metals* **2001**, *121*, 1467.
[18] V. L. J. Joly, P. A. Joy, S. K. Date, C. S. Gopinath, *J. Physics: Cond. Matt.* **2001**, *13*,649.
[19] C. J. Howard, H. Hunter, B. A. Rietica, *A Computer Program for Rietveld Analysis of X-Ray and Neutron Podwer Diffraction Patterns*, Australian Nuclear Science and Technology Organization Lucas Heights Research Laboratories.
[20] P. Lunkenheimer, T. Rudolf, A. Hemberger, S. Pimenov, S. Tachos, F. Lichtenberg, A. Loidl, *Phys. Rev B.* **2003**, *68*, 245108.
[21] H. Lixin, J. B. Neaton, M. H. Cohen, D. Vanderbilt, C. C. Homes, *Phys. Rev B.* **2002**, *65*, 214112.
[22] R. Viana, P. Lunkenheiner, J. Hemberger, R. Böhmer, A. Loidl, *Phys. Rev B.* **1994**, *50*,601.
[23] J. Ross Macdonald, LEVM version 8.0 Comlex Nonlinear Squares Fitting Program, 2003.
[24] Z. Yang, L. Ye, X. Xie, *Phys. Rev. B* **1999**, *59*, 7051.
[25] A. K. Jonscher, *Dielectric relaxation in solids*, Chelsea dielectric press, London, 1983.
[26] J. C. Maxwell, *Electricity and Magnetism*, Clarendon Press, Oxford, 1982.
[27] A. Von Hippel, *Dielectrics and Waves*, Artech House, Boston, 1995.
[28] J. T. S. Irvine, D. C. Sinclair, A. R. West, *Adv. Mater.* **1990**, *2*, 132.
[29] P. Lunkenheimer, V. Bobnar, A. V. Pronin, A. I. Ritus, A. A. Volkov, A. Loidl, *Phys. Rev. B* **2003**, *66*, 052105.
[30] A. Castro-Couceiro, M. Sánchez-Andújar, B. Rivas-Murias, J. Mira, J. Rivas, M. A. Señarís-Rodríguez, *Solid State Sci.*, in press.
[31] D. V. Efremov, J. Brink, D. I. Khomskii, cond-mat 0306651.

 © 2005 WILEY-VCH Verlag GmbH & Co. KGaA, 69451 Weinheim